Alma Mater Studiorum Università di Bologna
Archivio istituzionale della ricerca

Simulation of the Volt/Var Control in Distribution Feeders by Means of a Networked Multiagent System

(Article begins on next page)

23 February 2025

Simulation of the Volt/Var Control in Distribution Feeders by Means of a Networked Multiagent System

Riccardo Bottura, *Student Member, IEEE,* and Alberto Borghetti, *Senior Member, IEEE*

Abstract—The adoption of networked multiagent systems (MAS) has been recently proposed for the solution of the volt/var control (VVC) problem in distribution feeders. However, constraints and limitations due to the communication network, to the dynamic behavior of power system components and regulators, as well as to the measurement uncertainties of the adopted sensors need to be specifically analyzed for the design of the MAS. For this purpose, a cosimulation platform has been built by the integration of two simulation tools: 1) the electromagnetic transient program EMTP-rv; and 2) the communication network simulator Riverbed-OPNET Modeler. This paper presents the modeling and simulation of an asynchronous leaderless MAS-based approach that coordinates the reactive power outputs of a set of power compensators equipped with phasor measurement units via a shared band-limited packet-switched digital communication network. The effects of communication network latency and packet loss on the VVC performances are analyzed for two unbalanced IEEE Test feeders equipped with on-load tap changer transformers. The paper compares the results obtained by using a transmission control protocol (TCP) and a user datagram protocol (UDP), for different levels of background traffic (BT) and different packet discard ratios (PDRs) in the communication links.

Index Terms—Cosimulation, medium voltage distribution feeders, multiagent systems (MAS), networked control systems (NCS), phasor measurement unit (PMU), volt/var control (VVC).

I. INTRODUCTION

COSIMULATION environments that integrate a simulator of the communication network with a power system simulator are very useful for the design and analysis of improved monitoring, control, and protection techniques in modern electric power systems, as all these functions rely on the exchange of information using a shared communication network [1]. This approach appears particularly suitable for the development of active network management (ANM) functions of medium voltage (MV) networks that need to coordinate an increasing number of various type of spatially distributed energy resources and control devices by using communication networks characterized by more stringent limitations than those adopted for the operation of high voltage transmission networks [2].

As analyzed in [3], the implementation of all ANM functions in a central distribution management system (DMS) is expected

to require significant reinforcements of the communication infrastructures currently adopted by distribution network operators (DNOs). A reduction of the communication requirements can be obtained by using distributed approaches based on networked multiagent systems (MAS) composed by multiple local controllers interacting through the communication network. A general review of the applications of MAS in power systems, not limited to distributed control purposes, has been the object of a specific IEEE Power and Energy Society (PES) Working Group [4]. Control theory aspects, specifically consensus and cooperation topics, have been recently reviewed in [5].

These approaches avoid that all the information and decisions are concentrated in a specific node of the communication network connected to the centralized processor with demanding computational tasks. However, specific techniques of control over communication network are needed in order to minimize the effects of finite bandwidth, transmission delays, and packet loss, as well as to limit the cyber-attacks risk. These constraints due to the use of a shared communication network are common to all networked control systems (NCS) approaches as recently reviewed in [6] and [7].

Among the ANM functions, this paper focuses on the volt/var control (VVC), defined as the online coordination of reactive power resources and transformers equipped with on-load tap changers (OLTCs), in order to achieve an efficient and feasible operating condition of the power feeder. This paper does not directly deal with conservative voltage reduction (CVR). However, VVC tries to achieve flat voltage profiles along the feeder and, therefore, it facilitates the implementation of CVR projects.

Modern VVC approaches exploit the presence of distributed generators (DGs), especially of those connected to the power distribution feeder through power electronic converters, in addition to the classical control means such as OLTCs, mechanical switched capacitors, and static var compensators. Real power outputs of DGs are assumed to be defined by the availability of the energy resources and by market conditions.

VVC can be formalized as a single optimization problem as recently described, e.g., in [8] and [9], which also review previous contributions on the subject. Nevertheless, various distributed approaches have been also proposed in the literature for the solution of the VVC problem.

In [10], a decomposition method of the inverse of the Jacobian of the power flow problem is proposed in order to decompose VVC in smaller size optimization problems that could be implemented in MAS. There is also an increasing literature relevant to the application of distributed optimization procedures to VVC, with particular reference to power networks with radial structure (e.g., [11]–[14]).

In some MAS schemes, special coordinating roles are assigned to specific agents. As an example, in the scheme proposed in [15], a moderator collects all the sensitivity factors from the agents and sends backward the contracts to them stating that the amount of reactive power support is needed from each controlled DG. In [16], a similar coordinating role is attributed to a top feeder relay which has the additional role to provide the coordination with the central energy management system of the bulk transmission network. In other approaches, the sequence of agent actions should follow a specific order, based, as in, e.g., [17], on the location of the controlled DG in the feeder.

Moreover, leader-less MAS approaches have been recently proposed in [18] and [19]. These approaches are based on gossip-like algorithms that use the measurement of bus voltage synchrophasors and exchange the information between two randomly-chosen neighboring agents at a time. A related strategy has been presented in [20]. In [21], an algorithm is proposed in which each agent sets a target voltage value on the basis of the voltage measurements collected from all the neighbors. The action of each agent is cyclically activated by a token ring control strategy so as to ensure that the output of only one DG or of few DGs at a time is adjusted depending on the number of circulating tokens. In [22], the solution of a fuzzy-based algorithm is achieved by means of an average consensus procedure between agent state vectors. The results show that a large number of iterations and, therefore, a large number of exchanged messages are needed to achieve a consensus on the mean value of the bus voltages that is used by the fuzzy algorithm.

This paper aims at showing the application of an information and communications technology (ICT)-power system cosimulation platform to the analysis of the effects of the limitations of the communication links on the performances of a MAS approach and for the design of the relevant countermeasures.

As described in Section II, we focus on a leader-less asynchronous gossip-like approach given by subsequent repetition of the execution of simple rules between different couple of agents. The procedure, based on the one proposed in [18]–[20], is enriched by several countermeasures against communication latency and packet loss. It also incorporates additional heuristic rules that improve the coordination with OLTCs. Section III provides a step-by-step description of the implemented algorithm. Section IV describes the cosimulation platform that has been built by a means of an interface between the event-domain communication network simulator Riverbed-OPNET Modeler [23] and the time-domain power system simulation environment EMTP-rv [24]. Section V is devoted to the performance analysis of the procedure for the case of the IEEE 37-bus test feeder and of the IEEE 123-bus test feeder [25] with several agents, each controlling a reactive power compensator. The statistical results obtained by applying both a transmission control protocol (TCP) and a user datagram protocol (UDP) are compared for different levels of background data traffic and packet discard ratios (PDRs). Section VI concludes the paper.

II. GOSSIP-LIKE VVC PROCEDURE

Consensus algorithms in MAS can be described as rules that periodically update the column vector of the agent states $x(t + \Delta t)$ at time step $t + \Delta t$ by an exchange of information between the agents relevant to their present state

$$x(t + \Delta t) = \mathbf{P}(t)\, x(t). \tag{1}$$

Element P_{ij} of matrix $\mathbf{P}$ represents the influence of the present state of agent j on the future state of agent i at each time step. Therefore, matrix $\mathbf{P}$ incorporates the available communication links between different agents.

In the described VVC application, the state of agent i represents reactive power Q_i injected in a bus of the feeder by the reactive power compensator (based on a power electronic converter) supervised by the agent. As the objective of VVC is the achievement of a feasible and efficient operating condition, the updated value of the reactive power depends also on the state of the electrical network represented by the vector of bus voltage phasors V. Therefore, the consensus mechanism may be described by

$$Q(t + \Delta t) = Q(t) + \Delta Q(\mathbf{P}(t)\, V)$$
$$V(t) = f(Q(t),\, u(t)) \tag{2}$$

where ΔQ_i is the adjustment function of reactive power output of the compensator associate with agent i. It is a nonlinear function of the voltage phasors that are communicated to agent i by the available communication links represented by the nonzero elements of matrix $\mathbf{P}(t)$. Nonlinear function f represents the nonlinear relationship between the bus voltage phasors and the reactive power output of the compensators. It incorporates the power network equations, the voltage dependence of loads and generators as well as the effects of disturbances (switching, sudden load and generation changes, etc.) indicated by vector $u(t)$.

Among the various approaches that could be represented with the mechanism described by (2), this paper focuses to a gossip-like approach that avoids the synchronization of the action of the agents.

Although distributed optimization approaches, such as those presented in [11]–[14], are characterized, in general, by improved convergence behavior and quality of the results with respect to gossip-like algorithms, they entail stronger synchronization constraints between the actions of all the agents of the network, as well as more demanding communication requirements. The analysis of the effects of the limits of the communication network and the design of countermeasures against latency and packet loss in distributed optimization approaches is outside the scope of this paper.

The aspects that mainly characterize the implemented procedure are as follows.

1) Repetition of reactive power compensations between a couple of compensators, evaluated by using only the measurements available at the buses where the two compensators are connected.

2) Activation of different couples of compensators at each time, so as to limit the interference of the concurrent action of multiple compensators connected to the same feeder.

3) Robustness against communication latency and packet loss (at the limit, the procedure is expected to continue also in

the presence of the complete failure of a communication link).

A. Evaluation for the Reactive Power Compensation

Each agent updates the reactive power injected by its three phase compensator in a bus of the electric power feeder on the basis of the information received from the other agent, as well as by using the local information provided by a phasor measurement unit (PMU).

PMU applications for transmission system operation and control could be considered mature [26]. There is a growing interest to develop PMU-based applications also for distribution networks and PMUs are foreseen to be more commonly installed in future distribution equipment, as reviewed in [27] and references therein. The different characteristics of distribution feeders with respect to transmission grids justify the development of specific PMU algorithms. For example, in [28] and [29], a PMU prototype is described that addresses the issue of small phase shifts between different buses in distribution networks due to short line lengths and reduced power flows.

The principal aim of the action of each couple of agents that operates at each step of the procedure is the minimization of reactive power flows in the network. The minimization of the reactive power flows reduces the currents into overhead lines and cables, resulting in a reduction of losses and voltage drops. For this purpose, each couple of active agents tries to compensate the reactive power flow between them, i.e., each agent tries to supply the reactive power needed by the nearby loads.

In order to evaluate the amount of this reactive power counterflow to be generated by the two compensators, we assume the feeder as a balanced three-phase system. The single-phase equivalent positive circuit is replaced by a reduced network, the nodes of which are the substation bus (at the low-voltage side of the transformer) and the N busses at which the compensators are connected. The reduced $N + 1$ bus network is obtained by using the Kron's technique [30], [31].

As the feeder is unbalanced, the positive sequence admittance matrix $\mathbf{Y}$ is calculated by averaging the diagonal and off-diagonal values of the impedances matrices of unbalanced lines, by neglecting shunt capacitances.

According to the Kron's reduction technique the relationships between node current phasors $\boldsymbol{I}$ and voltage phasors $\boldsymbol{V}$ though matrix $\mathbf{Y}$ (assumed symmetrical) can be written as

$$\begin{bmatrix} \boldsymbol{I}_\alpha \\ \boldsymbol{I}_\beta \end{bmatrix} = \begin{bmatrix} \mathbf{Y}_{\alpha\alpha} & \mathbf{Y}_{\alpha\beta} \\ \mathbf{Y}_{\alpha\beta}^T & \mathbf{Y}_{\beta\beta} \end{bmatrix} \begin{bmatrix} \boldsymbol{V}_\alpha \\ \boldsymbol{V}_\beta \end{bmatrix} \tag{3}$$

where subscript α indicates the set of $N + 1$ nodes to be maintained in the reduced network, while subscript β denotes the other nodes. By applying the Gaussian elimination

$$\boldsymbol{I}_\alpha + \mathbf{Y}_{ac}\boldsymbol{I}_\beta = \mathbf{Y}_{\text{red}}\boldsymbol{V}_\alpha \tag{4}$$

with $\mathbf{Y}_{ac} = -\mathbf{Y}_{\alpha\beta}\mathbf{Y}_{\beta\beta}^{-1}$ and $\mathbf{Y}_{\text{red}} = \mathbf{Y}_{\alpha\alpha} - \mathbf{Y}_{\alpha\beta}\mathbf{Y}_{\beta\beta}^{-1}\mathbf{Y}_{\alpha\beta}^T$, being $\mathbf{Y}_{\beta\beta}$ not singular as there is at least one connection between a β-bus and an α-bus of the feeder.

The reduced network described by (4) exchanges the same real and reactive power with the external components through the α-nodes as the original system does. As far as $\boldsymbol{I}_\beta$ is independent on voltages, if $\boldsymbol{I}_\alpha$ could be modified so as to obtain a power loss drop in the reduced network, the same loss drop is achieved also in the original system. A power loss reduction is reasonably expected also in unbalanced feeders with loads that do not exactly maintain the same current phasor, in view of the limited bus voltage deviations expected in power distribution feeders (namely few percentage points for the amplitude deviation and very few degrees for phase deviation). This is supported by the simulation results presented in Section V that are obtained for two unbalanced test systems with loads with different voltage dependence: constant impedance, constant current, and constant power.

Indeed, as shown in [9], Cartesian coordinates variations $\Delta I_{L,k}^{\text{re}}$ and $\Delta I_{L,k}^{\text{im}}$ (in p.u.) of load current phasor at node k can be written as linear combinations of bus voltage variations ΔV_k^{re} and ΔV_k^{im} with respect to an initial voltage phasor equal to $1\mathrm{e}^{\mathrm{j}0}$ p.u:

$$\Delta I_{L,k}^{\text{re}} = G_{L,k}\,\Delta V_k^{\text{re}} - B_{L,k}\,\Delta V_k^{\text{im}}$$
$$I_{L,k}^{\text{im}} = G_{L,k}\,\Delta V_k^{\text{im}} + B_{L,k}\,\Delta V_k^{\text{re}} \tag{5}$$

for a load with constant admittance $Y_{L,k} = G_{L,k} + jB_{L,k}$;

$$\Delta I_{L,k}^{\text{re}} = |In_k|\Delta V_k^{\text{im}}\sin\varphi$$
$$\Delta I_{L,k}^{\text{im}} = |In_k|\Delta V_k^{\text{im}}\cos\varphi \tag{6}$$

for a constant current with $|In_k|$ root-mean-square (RMS) value and $\cos\varphi$ power factor;

$$\Delta I_{L,k}^{\text{re}} = -In_k^{\text{re}}\Delta V_k^{\text{re}} - In_k^{\text{im}}\Delta V_k^{\text{im}}$$
$$\Delta I_{L,k}^{\text{im}} = In_k^{\text{re}}\Delta V_k^{\text{im}} - In_k^{\text{im}}\Delta V_k^{\text{re}} \tag{7}$$

for a constant power load, where In_k^{re} and In_k^{im} correspond to the load real and reactive power requests in p.u. at $1\mathrm{e}^{\mathrm{j}0}$. Assuming a load with rated apparent power of 1 p.u. and 0.75 power factor, a voltage deviation of 5% for the amplitude and of 2° for the phase corresponds to a 6.2% maximum variation of the load current Cartesian coordinates.

In general, even if the feeder has a radial topology (as those considered in Section V) as usually preferred by DNOs, the reduced network may contain loops. However, if we consider two α-buses h and k so that there is not any other α-bus connected close to the path between them in the feeder (from now on buses h and k will be indicated as adjacent), the impedance between the corresponding two nodes of the reduced network is equal or very similar to the effective impedance of the path

$$Z_{\text{eff},hk} = R_{\text{eff},hk} + jX_{\text{eff},hk} = Z_{hh} + Z_{kk} - 2Z_{hk} \tag{8}$$

where Z_{hh}, Z_{kk}, and Z_{hk} are the (h,h)th, (k,k)th, and (h,k)th elements of impedance matrix $\mathbf{Z}$, obtained as the inverse of admittance matrix $\mathbf{Y}$ by assuming the substation as slack bus.

We assume that bus h and bus k are adjacent buses and each of them is equipped with a reactive power compensator. In order to estimate the adequate reactive power counter-flow, the two

agents calculate the following values of reactive power transfer both positive in the direction from h to k

$$Q'_{hk} = \frac{X_{\text{eff},hk}|V_h|^2}{|Z_{\text{eff},hk}|^2} - \frac{X_{\text{eff},hk}|V_h||V_k|}{|Z_{\text{eff},hk}|^2}\cos(\theta_h - \theta_k)$$
$$- \frac{R_{\text{eff},hk}|V_h||V_k|}{|Z_{\text{eff},hk}|^2}\sin(\theta_h - \theta_k) \qquad (9)$$

$$Q''_{hk} = -\frac{X_{\text{eff},hk}|V_k|^2}{|Z_{\text{eff},hk}|^2} + \frac{X_{\text{eff},hk}|V_h||V_k|}{|Z_{\text{eff},hk}|^2}\cos(\theta_k - \theta_h)$$
$$+ \frac{R_{\text{eff},hk}|V_h||V_k|}{|Z_{\text{eff},hk}|^2}\sin(\theta_k - \theta_h) \qquad (10)$$

where $|V_h|$ and $|V_k|$ are the RMS values, and θ_h and θ_k are the phases of the positive-sequence voltage synchrophasors V_h and V_k, respectively, measured by the two agents and exchanged between them through the communication network.

Each agent is assumed to know the values of the effective impedances between the bus where its compensator is connected and the adjacent α-buses where the compensators of the neighboring agents are connected.

In [18]–[20], it is shown that a sequence of repeated compensations of the mean value of (9) and (10) is globally convergent to the minimum network loss operating condition under some simplifying assumptions, namely that all the load consumptions and the DG power outputs are balanced and independent of voltage variations, all line impedances are balanced and have the same inductance/resistance ratio, voltage drops and phase variations between neighboring buses are limited, communication between agents is free from delays and information losses, and the behavior of power electronic converters is almost ideal.

B. Subsequent Activation of Couples of Agents

The environment to be controlled is characterized by scarcely predictable changes and unreliable exchange of information. The subsequent activation of couples of agents based on a random choice makes easier the overcoming of communication problems and the unavailability of a specific compensator. The activation of each updating process in the gossip asynchronous algorithm is typically represented by a Poisson process (e.g., [32]), i.e., by a random activation so that the time interval between consecutive activations has an exponential probability distribution and it is independent of previous time intervals. The activated agent randomly chooses another neighboring agent. The two agents exchange the information, apply the updating rules and change their state.

If the updating procedure is very fast, the probability of a concurrent activation of different couples of compensators is negligible. However, as both the communication and the action of the reactive power compensators require some time, in the implemented procedure each couple of active agents chooses the following couple to be activated. The implemented procedure limits the probability that an agent will be never activated as the following couple is chosen so as to avoid, if possible, those agents already involved in the procedure.

Only after a predefined long time (e.g., tens of minutes) in which an agent is never activated (e.g., due to the failure of a critical communication link), a spontaneous activation governed by a Poisson process with a large rate parameter is allowed.

The analysis presented in [20] shows the advantages of a multihop random selection of the agents on the convergence of the algorithm to the optimal operating point. However, the multihop procedure appears more vulnerable in presence of latency and packet loss than the implemented single-hop procedure in which the compensation is performed only by neighboring agents.

C. Countermeasures Against the Loss of Packets and Communication Latency

As a countermeasure against the loss of packets during the procedure of choice of the next couple of active agents, multiple concurrent processes might be initiated in order to avoid the block of the procedure. However, the convergence of the algorithm may be hindered by the presence of concurrent compensations. Therefore such a possibility is limited by assigning to each new process an increased priority index. Whenever an agent is involved in a process with a lower priority index than that of a previous process to which the same agent has participated, it stops the lower-priority-index process. This mechanism avoids the long permanence of multiple concurrent compensation processes.

The countermeasure against communication latency is based on the availability of a memory buffer at each agent. The memory buffer stores the PMU-provided phasor data with the relevant time tag. This memory allows each couple of agents to estimate the reactive power flow by using synchronous values of voltage phasors. Another countermeasure against excessive communication latency is provided by the definition of a maximum delay t_{wait} after which the procedure carries on with the choice of a new active agent, as described in Section III.

III. ALGORITHM

Summarizing, N reactive power compensators are assumed to be connected to different buses of the power distribution feeder with the capability to inject a controllable value of reactive power between minimum limit Q_{min} and maximum limit Q_{max}. The reactive power injection level is adjusted by an agent of the MAS connected to a node of the communication network. Each agent is equipped with a bus voltage sensor that incorporates the PMU function and with a memory buffer where it cyclically stores both the measured phasors and the corresponding measurement times for a predefined time interval equal to t_{wait}.

The algorithm corresponds to the repeated execution of the following steps (indicated as a compensation cycle).

A. Measurement, Information Exchange, and Calculation of ΔQ

1) An agent, which we denote as agent h, is assumed to be activated by another agent that also provides its updated priority index p_h as explained in the last steps.
2) Agent h randomly chooses a neighboring agent in the communication network, identified as agent k (by avoiding

the agent that has activated him, if there is another one available).

3) Agent h sends to agent k both the most updated values (present in the memory buffer) of $|V_h|$ and θ_h of the positive sequence voltage phasor of the bus to which its compensator is connected and the indication of corresponding measurement time t_{meas}. Moreover, it sends the identifier of bus h, value p_h equal to its priority index and the values of the margins between the current reactive output Q_h of its compensator and the relevant minimum and maximum limits, i.e., $\delta_h^{\max} = Q_{h,\max} - Q_h$ and $\delta_h^{\min} = Q_{h,\min} - Q_h$.

4) When agent k receives the information from agent h, it accepts the assignment only if p_h is not lower than its priority index, otherwise it denies the assignment by sending the relevant message to agent h that concludes the compensation process with priority p_h.

5) If agent k accepts the assignment, it updates its priority index, if necessary, and finds the bus voltage phasor V_k measured at t_{meas} stored in his memory buffer. It calculates Q'_{hk} and Q''_{hk}, by using (9) and (10). Moreover, analogously to agent h, it calculates reactive power margins $\delta_k^{\max}$ and $\delta_k^{\min}$ relevant to its compensator connected to bus k.

6) In order to define adjustment ΔQ of the compensator set point, agent k compares the value $\overline{Q_{hk}} = \min(|Q'_{hk}|, |Q''_{hk}|) \cdot \text{sgn}(Q'_{hk})$ with the maximum allowed variations of the reactive output of both compensators, i.e., $\delta_k^{\max}$, $\delta_k^{\min}$ and $\delta_h^{\max}$, $\delta_h^{\min}$:

$$\Delta Q = \max\big(\min\big(\overline{Q_{hk}}, \delta_k^{\max}, -\delta_h^{\min}\big), \delta_k^{\min}, -\delta_h^{\max}\big). \quad (11)$$

If Q'_{hk} and Q''_{hk} have different signs, then ΔQ is set equal to 0.

B. Implementation of ΔQ

7) Agent k changes the output of its compensator by adding ΔQ only if at least one of the following two conditions is met

$$\begin{aligned}\Delta Q > 0 \quad &\text{and} \quad |V_k| < V_{\max} \\ \Delta Q < 0 \quad &\text{and} \quad |V_k| > V_{\min}\end{aligned} \quad (12)$$

where $V_{\max}$ and $V_{\min}$ are two values a few percent higher and lower than bus voltage rated value, respectively, so as to define the voltage interval of the normal operating state. If none of (12) is met, the reactive power output is not changed.

8) Agent k sends back value ΔQ to agent h.

9) If agent h does not receive the message from agent k before t_{wait} after t_{meas}, it randomly selects another agent k (step 2). Priority index p_h remains unchanged.

10) If agent h receives the message from agent k, it changes the reactive output reference of its compensator by subtracting ΔQ only if at least one of the following two conditions is met

$$\begin{aligned}\Delta Q < 0 \quad &\text{and} \quad |V_h| < V_{\max} \\ \Delta Q > 0 \quad &\text{and} \quad |V_h| > V_{\min}.\end{aligned} \quad (13)$$

C. Selection of the New Couple of Agents

11) Agent h randomly chooses another agent to be activated as new agent h.

12) When the chosen agent receives the relevant message from agent h with the priority p_h, it checks whether p_h is greater or lower than its priority index. If it is equal or greater, the receiving agent becomes the new agent h. If necessary, it updates its priority index to p_h and sends the relevant acknowledgment message back to the old agent h, which then returns in the idle state. If p_h is lower than the priority index of the receiving agent, it denies the assignment by sending the relevant message to agent h that concludes the compensation process with priority p_h.

13) The new agent h starts again the procedure from step 1, waiting at least t_{wait} after t_{meas} so as to allow the stabilization of both compensators in the new operating conditions.

14) If the old agent h does not receive the acknowledgment message from the new one by t_{wait} after t_{meas}, it increments its priority index p_h and randomly selects another agent to be activated (step 11).

Conditions (12) and (13) exploit the fact that the connection to the transmission network through the substation transformer guarantees the reactive power balance in the feeder.

IV. ICT-POWER SYSTEM COSIMULATION PLATFORM

In this paper, an ICT-power system cosimulation platform is used to assess the performances of the described algorithm with a focus on the limitations due to a realistic model of the communication network.

In the literature, several approaches have been presented in order to develop ICT-power system cosimulation platforms, as recently reviewed in [2] and [33] (the latter also presents an event-driven cosimulation environment implemented in MATLAB/Simulink). One of the first platforms is the EPOCHS framework [34] that federates three off-the-shelf simulators: 1) PSCAD/EMTDC for power system transients; 2) positive sequence load flow (PSLF) for power system modeling; and 3) network simulator 2 (ns-2) for communication network modeling. The same type of simulators is also included in the GECO platform presented in [35] that uses a global event-driven mechanism in order to improve the synchronization. In [36], a cosimulation platform that integrates ns-2 with utility power distribution system simulator OpenDss is used to analyze a compensation scheme of photovoltaic arrays outputs by means of distributed storage units controlled through a wireless communication network. An OpenDss/ns-2 integrated tool is used also in [37] to evaluate the impact of WiMAX communication system characteristics (with particular reference to rain fade) on DMS advanced functions. In [38], various cosimulation architectures are described and applied to the analysis of a dc power distribution system in a ship-board application. One of these architectures, based on the link between OPNET and the dynamic model of power electronic devices developed by using the virtual test bed (VTB) software environment, is described in
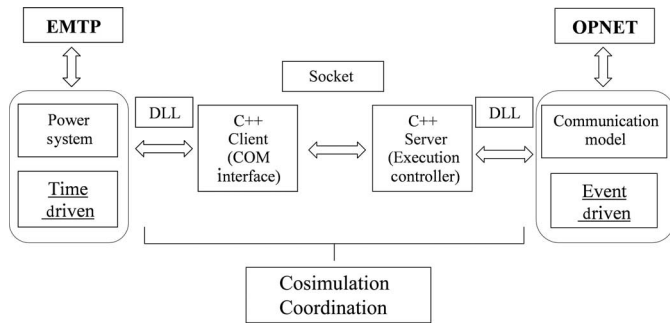
Fig. 1. Architecture of the cosimulation platform.

Fig. 2. Synchronization mechanism.

detail in [39]. In [40], a hybrid simulation design based on high level architecture (HLA), International Electrotechnical Commission Std. (IEC) 61850, object linking and embedding (OLE) for process control (OPC) and the common information model (CIM) is proposed with a focus on the evaluation of the real-time performance of wide-area monitoring, protection, and control (WAMPAC) applications. In [41], a cosimulation tool based on the interface between the eMEGAsim real-time digital simulator and OPNET is proposed for the development of PMUs applications. In [42], a cosimulation environment built using OMNeT++ and OpenDSS is presented and in [43], it is used to test an integrated vehicle-to-grid, grid-to-vehicle, and renewable energy sources coordination algorithm. Examples of more general cosimulation tools for cyber-physical systems applied to power networks are presented in, e.g., [44] (ADEVS/ns-2 integrated tool) and in [45] and [46] (Modelica/ns-2 integrated tool). Moreover, a review of cyber-physical system approaches in design and operation of power grids is available in [47].

As already mentioned, the developed platform is based on the interface between communication simulator OPNET and power system simulation environment EMTP-rv [48], [49]. As shown in Fig. 1, both OPNET and EMTP-rv communicate with the outside environment through dynamic link libraries (DLLs) specifically developed for this cosimulation platform. The DLLs communicate with each other through socket application programming interfaces (APIs). The socket API allows the developed DLL to control and use the network sockets that are the endpoints of the inter-process communication (IPC) flow.

In the socket communication, the OPNET controller works as a server (execution controller), while the EMTP-rv controller acts as a client. At the simulation start-up, OPNET enables the communication in the execution controller, opens a socket channel, sets the parameters, and starts to listening/waiting for a possible connection from the external environment. The co-simulation begins when the EMTP-rv sends the connection request as a client to the specific port and Internet protocol (IP) address provided by the server.

The synchronization mechanism between the two simulators is based on the typical waiting order of a communication through sockets. Simulation interval Δt is defined by the integration time-step adopted in EMTP-rv to solve the system of differential algebraic equations (for this paper, $\Delta t = 1$ ms). As illustrated in Fig. 2, Δt is communicated to OPNET that, in turn, executes the simulation until the subsequent sampling time $t + \Delta t$. As Δt is very small with respect to the analyzed transients, the inaccuracy
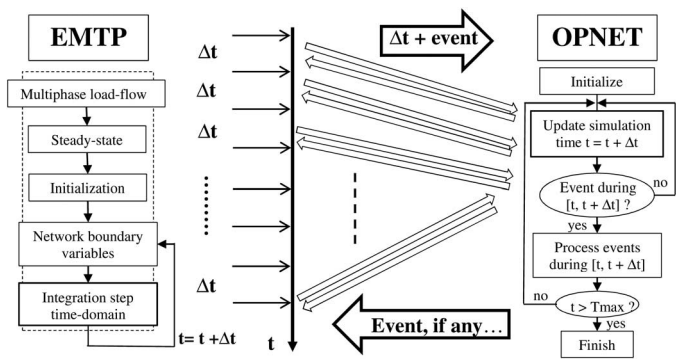
due to the time shift of all OPNET events that happen within a Δt interval to the end of the same interval is negligible.

A. Communication Model

A client–server communication model has been implemented for each OPNET–EMTP interface between a node of the communication network and the relevant agent that regulates a reactive power compensator implemented in the EMTP-rv model.

As described in [50] and [51], the OPNET interface through DLLs permits to use the OPNET GUI interfaces during the simulation and reduces the so-called memory swapping as the different functions of the simulator are loaded only when they are actually needed.

An OPNET DLL interface is defined by five main components: External system (Esys) module and the corresponding process model; external system definition/domain (ESD) model; simulation description (SD) file; Esys API package; external simulation access (ESA) API package. These components are briefly described below.

As illustrated in Fig. 3, both the TCP and UDP node models are extended by an Esys module that enables the management and the delivery of the communication packets. Each agent model in OPNET is composed by a client and a server in order to establish a point-to-point communication link.

ESD model is an attribute of the Esys module that defines an Esys interface for each agent. The Esys module uses the information contained in the SD file for the link to the OPNET DLL that includes the specific C/C++ functions defined by the Esys API package for the initialization and the flow control of each interface. The main header of the Esys API package is the ESA API package that contains the initialization of the sockets for the communication with EMTP-rv.

A message generated by the EMTP-rv model of the agents, implemented by using a specific DLL, is transferred at first to the socket communication and then to the relevant Esys interface of the client in the OPNET agent model. The message is built into the TCP or UDP datagram and sent to the server of the destination agent through the communication network. The destination server processes the received datagram, extrapolates the information from the payload, and returns the message to the associated EMTP-rv interface.

The TCP model establishes a connection-oriented point-to-point communication link and includes connection setup, data
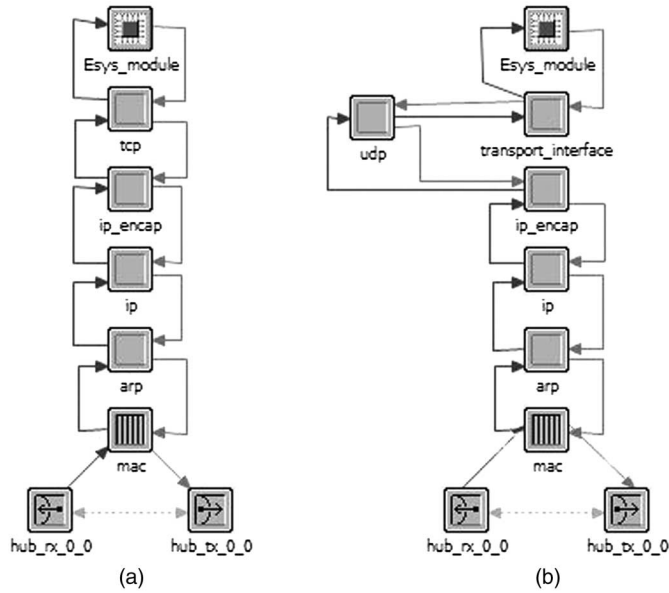
Fig. 3. (a) TCP and (b) UDP extended node models. hub_rx and hub_tx: physical layer; mac (Media Access Control) and arp (Address Resolution Protocol): link layer; ip (Internet Protocol) and ip_encap (which encapsulates packets into IP datagrams): internet layer; tcp or udp and transport_interface: transport layer.

exchange, acknowledgment, retransmission, and connection termination functionalities. In the UDP model, the communication is connectionless, i.e., a message is sent from one end point to another without prior arrangement or control. In our application, the dimension of TCP packets is 408 bits for data exchange and 376 bits for setup, acknowledgment and connection termination. The dimension of UDP packets is 312 bits.

In OPNET, each agent node is connected to a router and a background data traffic generator. The routers are connected to each other by a communication network with 64 kilobits per second (kbps) serial twisted-pair links. The network is characterized by a topology that follows the same tree configuration of the power distribution feeder. Each agent node is connected to the own router via a 10BaseT Ethernet link.

The background traffic (BT) in the communication links is represented by an IP layer traffic flow from each node towards the router located at the substation. Each communication link is also characterized by a PDR, representing the probability of a packet to be lost in the link.

B. Power Distribution Feeder Model

The EMTP-rv model of the network is mainly composed by the three-phase constant-parameters π-models for the representation of the unbalanced lines, a three-phase OLTC transformer model at the substation fed by a positive sequence constant voltage generator, the models of reactive power compensator, loads and other cascaded OLTC transformers.

The OLTC model is adapted from [52]. The OLTC regulator changes the tap when the RMS value of voltage at the secondary side differs from the reference value more than a predefined dead band for at least 0.5 s. The first tap change of each control action is postponed by a fixed delay, while subsequent changes are applied after a delay time fixed or with an inverse law. In order to avoid unnecessary operations and wear of the OLTCs of a

series of cascaded transformers, the upstream transformer sends a message to downstream transformers in order to delay their actions if those actions are of the same type of the one that the upstream transformer is applying [53]. Once the upstream transformer terminates its action, after t_{wait} it sends another message to downstream transformers in order to release their actions.

The compensators are represented by components able to inject assigned and adjustable three-phase active and reactive powers. A first approximation of the quasi-steady-state behavior of both synchronous generators and power electronic interfaced sources connected to an unbalanced network is provided by a three positive-sequence current sources in parallel with a 3×3 Y matrix (e.g., [54], [55]). The DG model implemented in EMTP-rv is composed by two positive-sequence triplets of current generators. The amplitude of one triplet is controlled by a feed-back regulator in order to inject the requested value of three-phase active power, while the phase angle between current and bus voltage is regulated so as to achieve a zero value of reactive power. The regulators of the second triplets have a reverse function, i.e., amplitude is controlled in order to inject the requested reactive power and phase angle is controlled in order to cancel out active injection. Reference value Q_i of the reactive power injection of compensator i is dynamically changed by the associated agent. A smooth transition between different power levels in a short time window of few hundreds of milliseconds is represented. The agent of each compensator includes also the model of a PMU that provides 10 estimates per second.

Each compensator i is equipped with a fast local controller that adjusts Q_i defined by the agent by a quantity $\Delta Q_{\text{local},i}$ in order to reduce Q_i if $|V_i| > V_{\text{max}}$ and to increase Q_i if $|V_i| < V_{\text{min}}$

$$\Delta Q_{\text{local},i} = -(|V_i| - V_{\text{max}})\frac{(-Q_{\text{min}} + Q_i)}{\Delta V_{\text{max}}}, \quad \text{if } |V_i| > V_{\text{max}}$$

$$\Delta Q_{\text{local},i} = (V_{\text{min}} - |V_i|)\frac{(Q_{\text{max}} - Q_i)}{\Delta V_{\text{max}}}, \quad \text{if } |V_i| < V_{\text{min}} \tag{14}$$

where ΔV_{max} indicates the transient voltage deviation that causes a complete utilization of the available reactive power margin.

As EMTP-rv converts all the load models to RLC branches in time-domain simulations, constant power and constant current three-phase unbalanced load models are represented by adopting the same two-triplets current-generators structure used for the compensators, with the difference that a per-phase control of active and reactive power (negative) injections has been implemented.

V. TEST RESULTS

Numerical tests have been carried out for the two following test feeders adapted from [25] with six additional three-phase reactive power compensators, indicated with Q1...Q6.

TF1: IEEE 37 Node Test Feeder, with the six reactive power compensators connected to buses 702, 712, 706, 703, 708, and 711, respectively (Fig. 4).

TF2: IEEE 123 Node Test Feeder, with the six reactive power compensators connected to buses 13, 28, 47, 67, 87, and 108, respectively (Fig. 5).
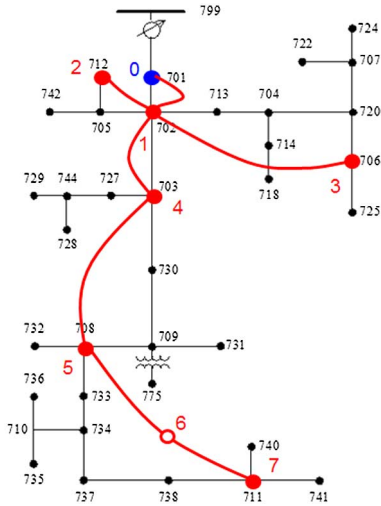
Fig. 4. TF1: power feeder in black and communication network in red. Red dots indicate the agents associated to compensators and the blue one indicates an agent that does not directly adjust the output of any compensator.
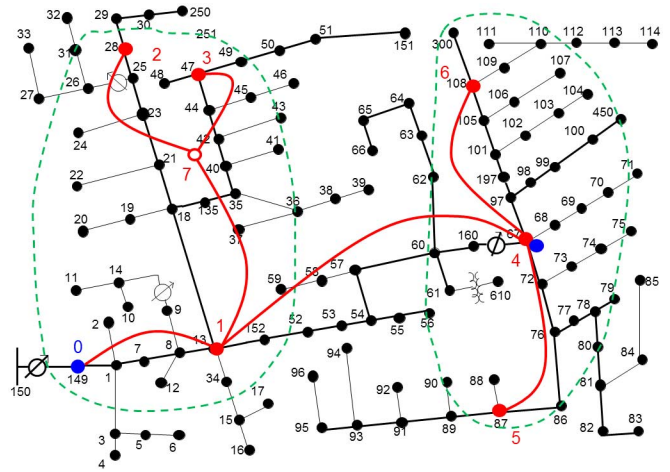

Fig. 5. TF2: power feeder in black and communication network in red. Red dots indicate the agents associated to compensators and the blue ones indicate agents that do not directly adjust the output of any compensator.

As a base case, limits Q_{max} and Q_{min} are set equal to 500 and -500 kvar, respectively, for all the compensators. The influence of more stringent limits (namely ± 250 and ± 150 kvar) has been also analyzed. Initially, the reactive power output of all the compensators is null.

The accuracy of PMUs is represented by the Normal distribution of the measurement errors. In the simulations, the corresponding mean and standard deviation values are assumed equal to 10 and 8.1 µrad for phase error and 120×10^{-6} and 9.3×10^{-6} p.u. for RMS error, respectively [29]. Also the accuracy associated with a capacitive voltage divider is included by means a Normal distribution with mean and standard deviation equal to -0.6 mrad and 7 µrad for the phase error and 2×10^{-3} and 58×10^{-6} p.u. for RMS error, respectively.

The characteristics of unbalanced lines and loads have been defined as in [25]. In order to speed up the simulations, the constant power and constant current load models described in Section IV-B have been applied only to the loads larger than 100 kW in TF1 and to the loads larger or equal than 40 kW in TF2, while the other loads are represented as constant impedances.

The procedure has also been applied to both the case of a higher load level and a lower load level than that indicated in [25]. The former (high load) is obtained by multiplying both the original active and reactive power values at each load bus (normal load) by a different number obtained by a uniformed distribution between 1.3 and 1.7. The latter (low load) is obtained by using multipliers uniformly distributed between 0.3 and 0.7.

Substation transformers are equipped with OLTC with ± 8 tap increments of 1.875%. The tap mechanical delay is 2 s, the time to first tap change is 20 s, and the maximum delay time of the subsequent tap changes is 15 s with an inverse law.

Three different BT levels are analyzed, identified as BT0, BT1, and BT2, which correspond respectively to 0, 4.75, and 9.5 kbps that each BT generator sends towards node 0. Each BT level is analyzed both without PDR (case identified as PDR0) and by assuming a 5% PDR (case identified as PDR5) for each communication link. For BT levels 0 and 1 we assume

$t_{wait} = 1$ s. For BT level 2, we have compared the results obtained for two t_{wait} values, namely $t_{wait} = 1$ s (BT2a) and $t_{wait} = 10$ s (BT2b). For the simulations with $t_{wait} = 1$ s, the final time is $t_f = 80$ s, when $t_{wait} = 10$ s t_f is extended to 100 s. In order to compare the promptness of the procedure in the various scenarios characterized by different BT levels, we define settling time t_{set} as the time to enter and remain within a 500 W band for at least 30 s. V_{max} and V_{min} are chosen equal to 1.03 and 0.97, respectively.

A. TF1

An ideal positive-sequence three-phase source is connected to the primary side of the substation transformer with line-to-line RMS value voltage equal to 230 kV. The rated ratio of the 2.5 MVA substation transformer is 230/4.8 kV with resistance $r = 2\%$ and reactance $x = 8\%$.

An additional agent is associated with bus 701, at the secondary side of the substation transformer. This agent participates to the regulation cycles of the VVC procedure but it does not directly adjust the output of any compensator.

As shown by Fig. 4, the wired communication network has 8 nodes with a tree topology that follows the same configuration of the power feeder: node 0 is located at the feeder substation (bus 701), nodes 1, 2, 3, 4, 5, and 7 connect the agents associated with the reactive power compensators, respectively, and node 6 is located in the path between node 5 and node 7. The communication network is therefore composed by 7 links: link 0 (nodes 0–1), link 1 (nodes 1–2), link 2 (nodes 1–3), link 3 (nodes 1–4), link 4 (nodes 4–5), link 5 (nodes 5–6), link 6 (nodes 6–7). Table I shows the BT percentage values in all the links for the considered three BT levels. Link 0 is the most affected by the traffic caused by the BT data flow concentration. The BT percentage value in link 0 produced by each BT generator is: 8.4% with 4.75 kbps and 16.7% with 9.5 kbps.

Tables II and III compare the results obtained for the seven scenarios characterized by different values of BT and PDR by using TCP and UDP with both OLTC and local controllers blocked. Since the gossip-like procedure is based on the random choice of the active agents, the tables report the results of the

TABLE I
BT LEVELS AND CORRESPONDING BT PERCENTAGE VALUES FOR EACH OF THE LINKS OF THE COMMUNICATION NETWORK OF TF1

BT levels	BT (%)					
	Link 0	Link 1	Link 2	Link 3	Link 4	Link 5 & 6
BT0	0	0	0	0	0	0
BT1	49.7	8.4	8.4	25	16.8	8.4
BT2	98.7	16.7	16.7	49.5	33.1	16.7

TABLE II
MEAN AND STANDARD DEVIATION VALUES OF THE NUMBER OF COMPENSATION CYCLES, PERCENTAGE OF INCOMPLETE COMPENSATIONS, POWER LOSS DECREASE, AND SETTLING TIME FOR TF1

BT PDR level	No of compensation cycles mean (stdev)		% of incomplete compensations mean (stdev)		Power loss decrease (kW) mean (stdev)		Settling time (s) mean (stdev)	
	TCP	UDP	TCP	UDP	TCP	UDP	TCP	UDP
BT0 PDR0	70.5 (0.5)	75.8 (0.4)	0 (0)	0 (0)	13.4 (0.1)	13.5 (0.1)	26.0 (13.0)	28.3 (10.9)
BT1 PDR0	68.2 (0.5)	74.5 (0.5)	0 (0)	0 (0)	13.4 (0.2)	13.5 (0.1)	26.0 (10.6)	23.1 (13.5)
BT2a PDR0	59.2 (1.9)	63.4 (1.9)	0 (0)	0 (0)	8.2 (3.1)	7.9 (3.0)	32.8 (19.3)	31.6 (23.5)
BT2b PDR0	9.5 (0.6)	10.0 (0.1)	0 (0)	0 (0)	10.6 (2.5)	11.5 (1.4)	–	–
BT0 PDR5	30.6 (11.8)	67.9 (5.3)	32.3 (11.5)	6.1 (2.7)	12.1 (1.9)	13.0 (2.1)	33.5 (21.9)	28.1 (12.9)
BT2a PDR5	35.4 (5.1)	58.3 (3.8)	29.0 (10.3)	7.3 (3.8)	10.9 (3.3)	10.7 (3.1)	33.3 (15.3)	33.8 (19.3)
BT2b PDR5	7.4 (1.3)	9.2 (1.6)	11.8 (14.8)	5.0 (6.4)	9.8 (2.4)	10.7 (2.8)		

TABLE III
MEAN AND STANDARD DEVIATION VALUES OF THE NUMBER OF PACKETS, PERCENTAGE OF IGNORED AND LOST PACKETS, PACKET DELAY, AND NUMBER OF STOPPED PROCESSES FOR TF1

BT (PDR) level	No. of packets mean (stdev)		% of packets ignored or lost mean (stdev)		% of packet lost mean (stdev)	Packet delay (ms) mean (stdev)		No. of stopped processes mean (stdev)	
	TCP	UDP	TCP	UDP	UDP	TCP	UDP	TCP	UDP
BT0 PDR0	282.0 (1.9)	303.2 (1.5)	0 (0)	0 (0)	0 (0)	49 (14)	11 (3)	0 (0)	0 (0)
BT1 PDR0	272.7 (1.7)	297.9 (1.9)	0 (0)	0 (0)	0 (0)	66 (33)	18 (16)	0 (0)	0 (0)
BT2a PDR0	245.9 (4.9)	264.4 (5.6)	4.2 (1.2)	4.2 (0.8)	0 (0)	76 (39)	22 (21)	0 (0)	0 (0)
BT2b PDR0	37.8 (2.5)	39.9 (0.5)	0 (0)	0 (0)	0 (0)	462 (918)	194 (523)	0 (0)	0 (0)
BT0 PDR5	188.6 (15.1)	276.1 (18.8)	47.2 (18.6)	5.7 (1.5)	5.7 (1.5)	52 (36)	12 (3)	2.6 (1.5)	1.8 (1.3)
BT2a PDR5	186.8 (7.3)	247.9 (10.6)	34.4 (6.6)	9.8 (1.5)	6.3 (1.4)	93 (88)	24 (33)	4.3 (1.8)	1.7 (1.3)
BT2b PDR5	30.7 (4.2)	37.7 (6.1)	11.2 (11.0)	4.5 (4.1)	4.5 (4.1)	890 (1509)	241 (561)	0.3 (0.6)	0.3 (0.6)

statistical analysis carried out by performing 30 simulations for the same case. For each simulation, the pseudorandom number generator is initialized by a different seed state associated with the computer system time. In Table II, the number of compensation cycles is the number of cycles in which at least one compensator changes its reactive power and the percentage of incomplete compensations indicates the percentage of cycles that do not complete regularly; the power loss decrease indicates the difference between the values of power losses at the starting time and at t_{set}. In Table III, the number of packets takes into account only the packets carrying the compensation data sent by the agents; the percentage of ignored or lost packets refers to those that arrive at destination after t_{wait} or do not arrive at all (for UDP the specific percentage of the lost packets is also provided); packets delay indicates the travelling time of the packets that regularly arrive at destination before t_{wait}; the number of stopped process is the number of stopping actions on the basis of the priority index value. The packet delay values indicated in Table III are the mean values of the statistical parameters obtained for each of the 30 simulations.

For BT0-PDR0, the mean value (standard deviation) in kvar of the final reactive power outputs of the six compensators is: 146.5 (25.6), 63.1 (2.2), 148.2 (1.4), 144.7 (7.6), 169.8 (4.0), and 164.7 (1.6). The limited values of the standard deviations show that the reactive output scheduling at the end of different compensation cycles is almost the same. The significant value of the first standard deviation is due to the location of compensator Q1 close to the slack bus. The low value of the standard deviation relevant to the loss decrease (fractions of a kilowatts) also

indicates that an analogous power flow conditions is achieved at the end of different sequence of compensations. The procedure converges in less than 30 s to a mean value of the final power losses of about 76.3 kW. The reduction of nearly 13.5 kW is in agreement with the results shown in [20]. Despite the significant differences between the two approaches, the results are also in reasonable agreement with those obtained by applying the three-phase version of the mixed integer linear programming (MILP) model proposed in [9] to the same distribution system. The solution of the MILP model provides the following reactive power scheduling (in kvar): 140, 75, 150, 140, 170, and 170 (in the implemented MILP model the reactive power outputs can be changed in steps of 5 kvar). The minimum power loss calculated by the MILP model is 76.27 kW, only some tens of watts lower than that achieved by the gossip procedure.

As shown in Tables II and III similar results are obtained also for case BT1-PDR0.

For the cases without packet loss (PDR0), as expected, the results show larger delays for increasing BT levels from 0 to 2. Even without PDR, in scenario BT2a, due to the congestion of the communication links, several packets do not reach the expected receiver within $t_{wait} = 1$ s and, therefore, they are ignored. Table III shows that in BT2b this problem is solved as t_{wait} is extended to 10 s. Whereas for $t_{wait} = 1$ s the compensation procedure is fast enough so that t_{set} could be considered the time at which the procedure converges, this is no longer true for BT2b. Therefore, for BT2b, the power loss decrease is evaluated at $t_f = 100$ s, although the convergence is not yet reached due to the insufficient number of compensation cycles.

For the cases with PDR = 5% (PDR5), the number of compensation cycles reduces, in particular, for TCP. The PDR causes an incomplete cycle when there is the loss of the packet that carries the information from agent k, which compensates first, to agent h. Moreover, the loss of the return packet from the new agent h and the old one causes the start of a process with increased priority index, as described in Section III. The presence

TABLE IV
POWER LOSS REDUCTIONS OBTAINED FOR TF1 AND DIFFERENT LOAD LEVELS

Load level	Initial power loss (kW)	Power loss decrease (kW)			
		BT0-PDR0		BT2-PDR5	
		TCP	UDP	TCP	UDP
Normal load	89.8	13.5	13.5	11.8	12.9
Low load	25.2	3.9	3.9	3.4	3.8
High load	211.8	31.1	31.1	24.6	28.0

Fig. 7. Variations of reactive power outputs of the compensators in TF1 for BT1-PDR0 case with UDP.
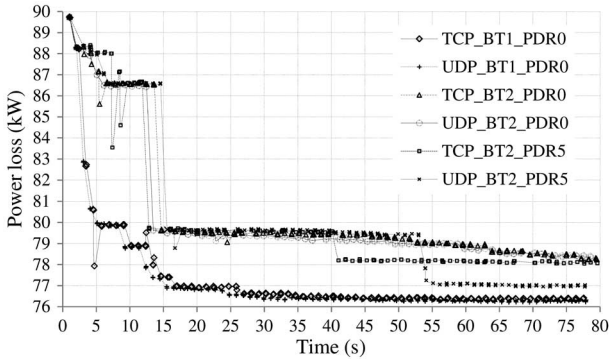
Fig. 6. Power loss variation in TF1 for different BT levels and PDR by using TCP and UDP.

Fig. 8. Bus voltage variations in TF1 for BT1-PDR0 case with UDP.

of concurrent processes is then eliminated by the stop of the process with lower priority index.

We could distinguish between lost packets because of PDR5 from those ignored due to excessive delay only by using UDP, while this classification is not possible with the implemented TCP model because it closes the communication after t_{wait}.

The comparison between BT2-PDR0 and BT2-PDR5 cases shows that packet loss due to PDR5 partially attenuates the effect of the high BT level, especially in link 0. As a consequence, Table II shows that the mean power loss decrease value is higher in BT2-PDR5 than in BT2-PDR0.

As already described, two other load levels have been analyzed, one higher and one lower than the normal one. The results have been obtained by using the same seed state for the random number generation, i.e., by the same sequence of active agent pairs. The convergence of the procedure is similar for all the load levels and the obtained reductions of power losses are shown in Table IV for both BT0-PDR0 and BT0-PDR5.

Figs. 6–8 illustrate the time behavior obtained by the same sequence of active agents (i.e., determined by the same initial seed of random number generation) for the two different communication protocols and different network conditions. The feeder has normal load level and the OLTC at the substation is blocked at tap position 0. Fig. 6 compares the feeder power loss for cases BT1-PDR0, BT2-PDR0, and BT2-PDR5, by using TCP and UDP. Fig. 6 shows that the VVC action with TCP is slightly delayed with respect to the one obtained by using UDP. Moreover, while for the case BT1-PDR0 (which represents a medium utilization level of the communication links without PDR) all the compensation cycles are completed, for BT2-PDR0 and BT2-PDR5 some cycles cannot be completed. This justifies the reduced level of obtained efficiency. Fig. 7 shows the reactive
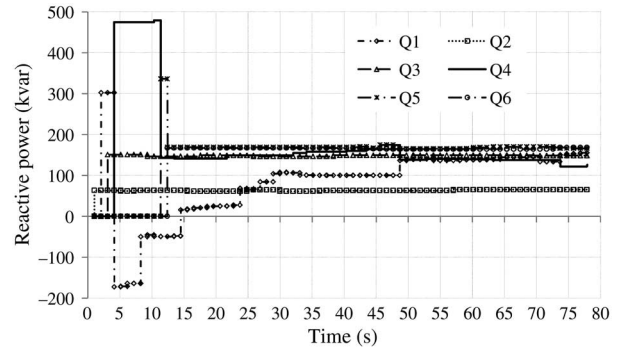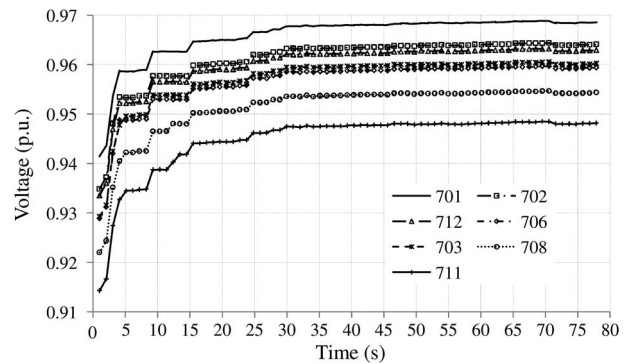
power outputs of the various compensators during the process and Fig. 8 shows the positive-sequence voltage RMS values measured by the agents for a case with efficient communication.

The coordination between the VVC procedure and the action of the OLTC at the substation is illustrated in Fig. 9 and Fig. 10. The value of the desired regulated voltage at the secondary side is 1.02 p.u. with a dead band limit of ± 0.015 p.u. The results show that in BT2-PDR5 cases the OLTC starts in tap position 0, operates a first tap change at 22 s and, after other 2 changes, reaches a final tap equal to -3 at 40 s. In BT1-PDR0 cases, the OLTC operates the first tap change at the same time and after one additional change reaches a steady-state condition at tap -2 at 30 s. The improved action by the agents with efficient communication results in a lower OLTC regulation. The increase of the power losses after each tap change is due to the increased consumption of voltage dependent loads.

Fig. 11 and Fig. 12 compare the results obtained by using the MAS procedure with those obtained by using the local controllers of the compensators described by (14) with $\Delta V_{max} = 0.3$ p.u. Fig. 11 compares the power loss decrease and Fig. 12 compares the voltage behavior at buses 701 and 711 calculated: 1) by using the MAS procedure without local controllers; 2) by using only the local controllers; and 3) by using the MAS procedure with the local controllers activated. The local controllers provide a first and fast action after a sudden perturbation, while the MAS procedure acts as a secondary regulation with the aim to achieve a more efficient utilization of the available resources.
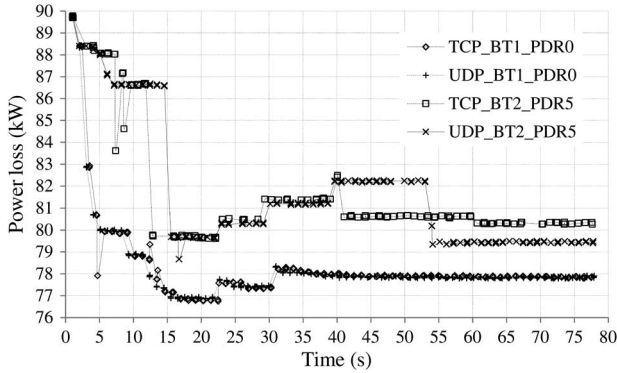
Fig. 9. Power loss variation in TF1 with active OLTC for different BT levels and PDR by using TCP and UDP.
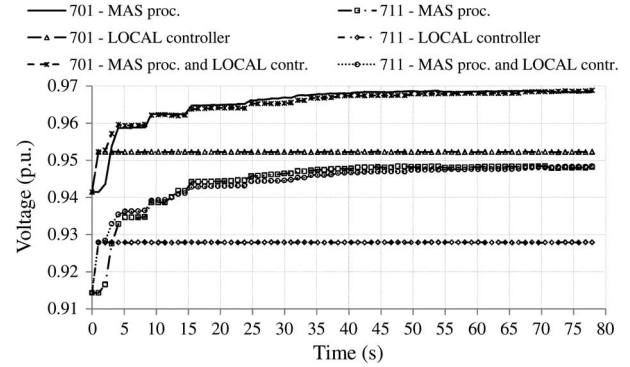

Fig. 10. Bus voltage variations in TF1 with active OLTC for case BT1-PDR0 with UDP.

Fig. 11. Comparison of power loss variation in TF1 with blocked OLTC by using the MAS procedure, by using only the local controllers, and by using both regulations (case BT1-PDR0 with UDP).
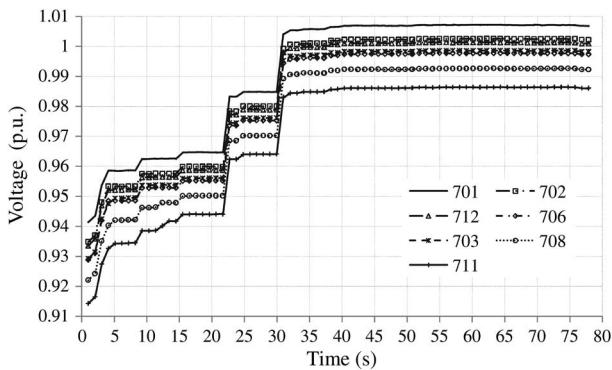
Fig. 13 compares the power loss decrease obtained by using the ± 500 kvar compensators with the results obtained by using smaller-size compensators: ± 250 and ± 125 kvar. The final reactive power scheduling in kvar of the six compensators is: 136.19, 64.74, 146.84, 147.55, 168.89, 164.71 (± 500 kvar); 131.53, 66.15, 148.62, 165.65, 170.44, 165.85 (± 250 kvar); and 125, 65.39, 125, 125, 125, 125 (± 125 kvar). Both the ± 500 and ± 250 limits are not binding; therefore the same 13.5 kW final loss reduction is achieved. The ± 125 limits bind the optimal solution of 5 compensators causing a reduction of the power loss decrease to 12.7 kW.

Fig. 12. Comparison of bus voltage variations in TF1 with blocked OLTC by using the MAS procedure, by using only the local controllers, and by using both regulations (case BT1-PDR0 with UDP).
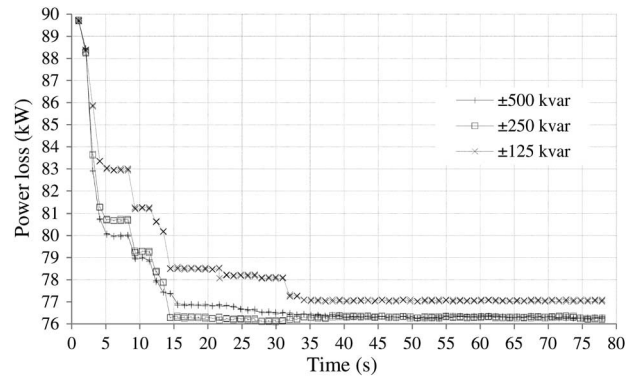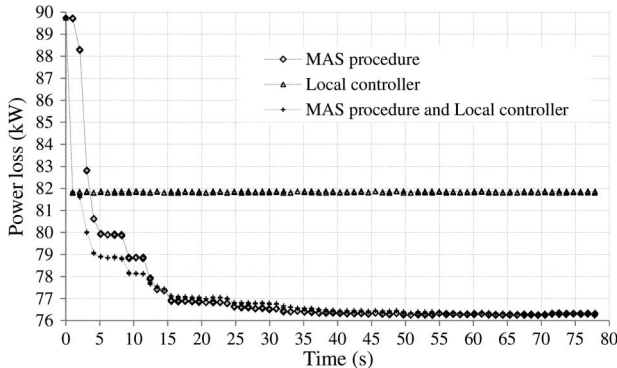

Fig. 13. Comparison of power loss variation in TF1 with blocked OLTC by using compensators of different sizes (case BT1-PDR0 with UDP).

B. TF2

The ideal positive-sequence three-phase source connected to the primary side of the substation transformer has line-to-line RMS value voltage equal to 115 kV. The rated ratio of the five MVA substation transformer is 115/4.16 kV with $r = 1\%$ and $x = 8\%$. Agent 0, associated with bus 701 at the secondary side of the substation transformer, participates to the regulation cycles of the VVC procedure but it does not directly adjust the output of any compensator.

The transformer located between bus 160 and 67 has an OLTC with ± 16 tap increments of 0.625%. The time to first change and the maximum time of subsequent-changes inverse-law delay are both 10 s and the mechanical delay is 2 s.

As shown in Fig. 5, the communication network has eight nodes with a tree topology: node 0 is located at the feeder substation (bus 149), nodes 1, 2, 3, 4, 5, and 6 connect the agents associated with the reactive power compensators, respectively, and node 7 is located in the path between nodes 1, 2, and 3. The communication network is, therefore, composed by 7 links: link 0 (nodes 0–1), link 1 (nodes 1–7), link 2 (nodes 7–2), link 3 (nodes 7–3), link 4 (nodes 1–4), link 5 (nodes 4–5), and link 6 (nodes 4–6). Table V shows the BT percentage values in all the links for the considered three BT levels. The BT percentage value in link 0 produced by each BT generator is: 8.4% with 4.75 kbps and 16.5% with 9.5 kbps.

Agent 4 controls the reactive power compensator connected to bus 67 only when the OLTC between bus 160 and 67 is not

TABLE V
BT LEVELS AND CORRESPONDING BT PERCENTAGE VALUES FOR EACH OF THE LINKS OF THE COMMUNICATION NETWORK OF TF2

BT level	BT (%)				
	link 0	link 1	link 2 & 3	link 4	link 5 & 6
BT 0	0	0	0	0	0
BT 4.75	49.0	16.5	8.4	24.8	8.4
BT 9.5	98.2	33.0	16.5	49.3	16.5

TABLE VI
MEAN AND STANDARD DEVIATION VALUES OF THE NUMBER OF COMPENSATION CYCLES, PERCENTAGE OF INCOMPLETE COMPENSATIONS, POWER LOSS DECREASE, AND SETTLING TIME FOR TF2

BT (PDR) level	No of compensations cycles mean (stdev)		% No. of incomplete compensations mean (stdev)		Power loss decrease (kW) mean (stdev)		Settling time (s) mean (stdev)	
	TCP	UDP	TCP	UDP	TCP	UDP	TCP	UDP
BT0 PDR0	70.7 (0.7)	77 (0.0)	0 (0)	0 (0)	11.4 (0.2)	11.4 (0.1)	24.7 (13.5)	21.0 (11.6)
BT1 PDR0	68.1 (0.8)	75.9 (0.4)	0 (0)	0 (0)	11.4 (0.2)	11.4 (0.2)	26.2 (12.6)	18.9 (12.9)
BT2a PDR0	59.1 (2.3)	65.5 (1.8)	0 (0)	0 (0)	8.9 (2.8)	8.9 (2.3)	30.3 (16.0)	34.8 (21.2)
BT2b PDR0	9.3 (0.7)	10.0 (0.2)	0 (0)	0 (0)	9.9 (2.2)	10.6 (1.4)	–	–
BT0 PDR5	32.6 (10.0)	65.7 (6.3)	34.8 (11.0)	7.2 (3.7)	10.8 (1.3)	11.3 (0.5)	31.7 (18.5)	26.4 (15.6)
BT2a PDR5	32.8 (5.1)	56.0 (10.4)	28.1 (8.3)	8.1 (4.1)	9.3 (2.2)	9.9 (2.0)	34.6 (20.0)	39.2
BT2b PDR5	7.3 (1.9)	8.6 (1.0)	11.4 (11.4)	5.1 (7.9)	8.1 (2.6)	9.3 (2.6)	–	–

TABLE VII
MEAN AND STANDARD DEVIATION VALUES OF THE NUMBER OF PACKETS, PERCENTAGE OF IGNORED AND LOST PACKETS, PACKET DELAY, AND NUMBER OF STOPPED PROCESSES FOR TF2

BT (PDR) level	No. of packets mean (stdev)		% of packets ignored or lost mean (stdev)		% of packet lost mean (stdev)	Packet delay (ms) mean (stdev)		No. of stopped processes mean (stdev)	
	TCP	UDP	TCP	UDP	UDP	TCP	UDP	TCP	UDP
BT0 PDR0	282.5 (2.5)	308.0 (0.1)	0 (0)	0 (0)	0 (0)	61 (19)	15 (5)	0 (0)	0 (0)
BT1 PDR0	271.7 (2.9)	303.5 (1.7)	0 (0)	0 (0)	0 (0)	83 (33)	22 (17)	0 (0)	0 (0)
BT2a PDR0	244.6 (7.3)	271.7 (5.4)	3.6 (1.1)	3.5 (0.7)	0 (0)	98 (43)	29 (24)	0 (0)	0 (0)
BT2b PDR0	36.8 (2.9)	39.9 (0.7)	0 (0)	0 (0)	0 (0)	629 (1078)	184 (513)	0 (0)	0 (0)
BT0 PDR5	188.0 (14.9)	273.8 (25.3)	44.5 (17.0)	6.8 (1.4)	6.8 (1.4)	63 (35)	15 (5)	2.8 (1.8)	2.9 (1.7)
BT2a PDR5	185.0 (10.9)	240.2 (43.8)	38.7 (8.0)	10.2 (1.4)	7.2 (1.9)	99 (66)	30 (36)	3.7 (1.6)	2.6 (1.3)
BT2b PDR5	30.6 (4.5)	36.1 (3.0)	13.7 (15.4)	6.4 (4.1)	6.4 (4.1)	814 (1355)	162 (413)	0.2 (0.4)	0.4 (0.7)

TABLE VIII
POWER LOSS REDUCTIONS OBTAINED FOR TF2 AND DIFFERENT LOAD LEVELS

Load profile	Initial power loss (kW)	Power loss decrease (kW)			
		BT0-PDR0		BT2b-PDR 5	
		TCP	UDP	TCP	UDP
Normal load	125.8	11.4	11.4	11.2	11.3
Low load	33.0	1.05	1.06	1.03	1.03
High load	300.0	43.2	43.2	40.0	42.5

operating. When the OLTCs are in operation, the agents are divided into two groups, namely {0,1,2,3} and {4,5,6} as shown in Fig. 5, so that at each compensation cycle both agent h and agent k must belong to the same group. Moreover, agent 0 sends a message to agent 4 when the voltage at the secondary side of the substation transformer leaves the dead band. This message increases the tap delay of the downstream OLTC of 120 s. Once the voltage returns inside the dead band, after t_{wait} agent 0 sends a reset message to agent 4.

Tables VI and VII compare the results of the statistical analysis relevant to 30 simulations for all the scenarios already defined for TF1. The random number generators are initialized by different seed states. Both OLTCs are blocked in tap position 0.

For BT0-PDR0 case, the mean value (standard deviation) in kvar of the final reactive power outputs of the six compensators is: 258.2 (67.7), 154.2 (2.3), 421.1 (2.3), 272.4 (56.2), −88.6 (17.0), 132.7 (5.9). As for TS1, also for TS2, a very small value of the standard deviation of loss decreases is obtained. It indicates that analogous power flow conditions are achieved at the end of different sequence of compensations.

Table VIII compares the loss reductions obtained for normal load, low load and high load conditions by assuming BT0-PDR0 and BT0-PDR5 communication conditions with both OLTCs blocked in tap position 0.

The sequence of compensations is illustrated by Fig. 14 and Fig. 15 with both OLTCs blocked in tap position 0 and by Fig. 16 and Fig. 17 with both OLTCs in operation. For the latter case, the reference values of the secondary side voltage are: 1.01 p.u. for the substation transformer and 1 p.u. for OLTC transformer at bus 67, respectively, both with a dead band of ±0.015 p.u. In the
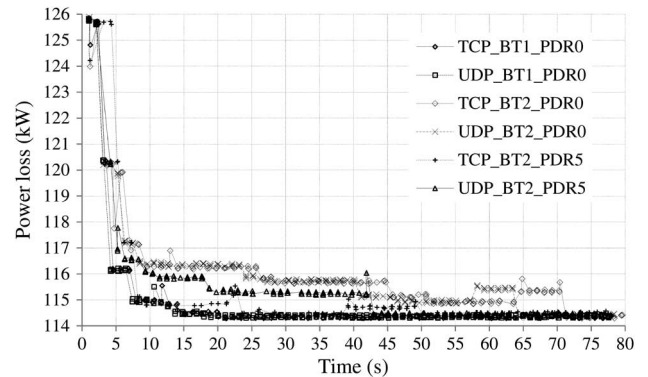

Fig. 14. Power loss variation in TF2 with blocked OLTCs for two different BT and PDR levels by using TCP and UDP.

simulation relevant to Fig. 16 and Fig. 17, the substation transformer changes the tap to −1 position at 22 s and reaches the steady-state condition. For BT1-PDR0 case with both TCP and UDP, OLTC transformer at bus 67 changes the tap to −1 at 25.6 s and then at about 35.6 s, reaching the final tap −2. For BT2-PDR5 case with UDP, this OLTC after the first tap variation at 25.6 s changes again 2 other times, reaching the steady-state condition to –3 at 44.8 s. For BT2-PDR5 case with TCP, the high BT level hinders the communication between agent 0 and agent 4. Therefore, the OLTC transformer at bus 67 anticipates the first change to nearly 12 s, and it reaches the steady-state condition with tap −4 at time 39.1 s after three other changes.
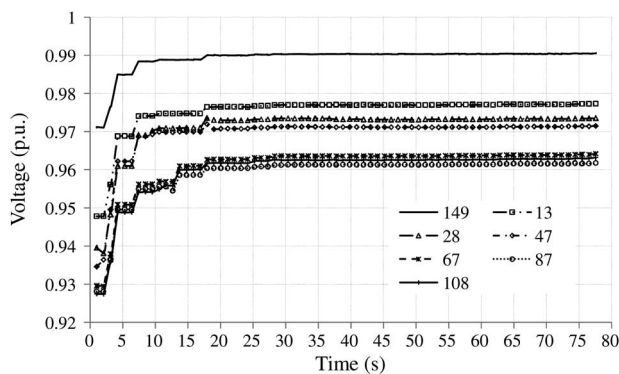
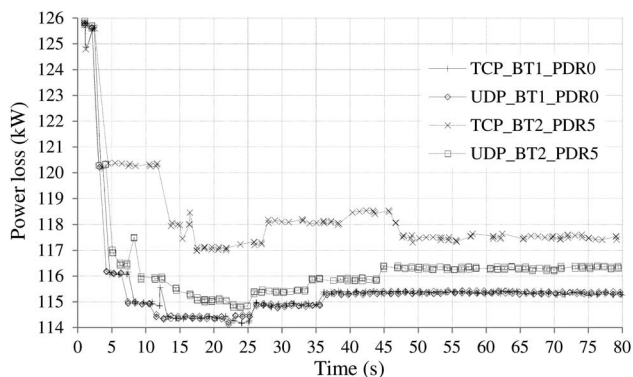Fig. 15. Voltage variations in TF2 with blocked OLTCs for BT2 by using UDP.

Fig. 16. Power loss variation in TF2 with the OLTCs in operation for two different BT levels by using TCP and UDP.
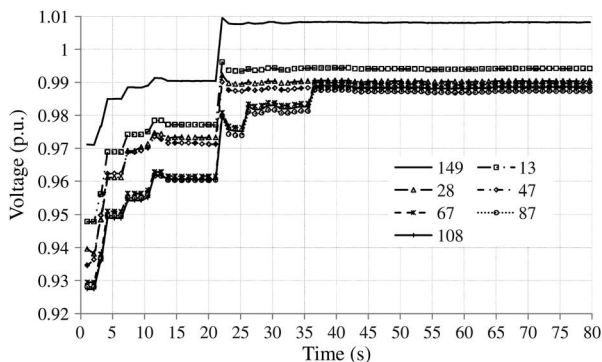

Fig. 17. Voltage variations in TF2 with the OLTCs in operation for BT1 by using UDP.

VI. CONCLUSION

The paper deals with the application of a specifically developed ICT-power cosimulation platform to the analysis of a leaderless multiagent system scheme for the VVC of distribution feeders with several reactive power compensators and also transformers equipped with OLTC.

The paper presents the mechanisms introduced in the adopted gossip-like algorithm in order to improve its robustness against the limitations induced by BT and packet loss in the communication channels. In particular, a mechanism based on a priority index has been implemented to allow for the start of multiple concurrent compensations processes whenever packets carrying critical information are lost. The processes with low priority indexes are progressively stopped by the agents in order to facilitate the convergence of the algorithm.

Although the algorithm assumes a balanced three-phase representation of the distribution feeder, the paper presents its application to test systems characterized by unbalanced lines and loads. The obtained results show that the performances of the adopted approach appear reasonably good also for medium values of background data traffic and PDR taking into account the accuracy of phasor measurements.

Moreover, a comparison between TCP and UDP is presented for different feeders and load conditions in order to analyze the effects on the control performances. Due to the specific countermeasure implemented against packet loss, the statistical analysis of the results shows that the use of UDP is in general to be preferred for this application.

REFERENCES

[1] Y. Yan, Y. Qian, H. Sharif, and D. Tipper, "A survey on smart grid communication infrastructures: Motivations, requirements and challenges," *IEEE Commun. Surveys Tuts.*, vol. 15, no. 1, pp. 5–20, Jan. 2013.
[2] K. Mets, J. A. Ojea, and C. Develder, "Combining power and communication network simulation for cost-effective smart grid analysis," *IEEE Commun. Surveys Tuts.*, Mar. 2014, to be published.
[3] Q. Yang, J. A. Barria, and T. C. Green, "Communication infrastructures for distributed control of power distribution networks," *IEEE Trans. Ind. Informat.*, vol. 7, no. 2, pp. 316–327, May 2011.
[4] S. D. J. McArthur *et al.*, "Multi-agent systems for power engineering applications—Part I: Concepts, approaches, and technical challenges," *IEEE Trans. Power Syst.*, vol. 22, no. 4, pp. 1743–1752, Nov. 2007.
[5] Y. Chen, J. Lu, X. Yu, and D. J. Hill, "Multi-agent systems with dynamical topologies: Consensus and applications," *IEEE Circuits Syst. Mag.*, vol. 13, no. 3, pp. 21–34, third quarter 2013.
[6] R. A. Gupta, "Networked control system: Overview and research trends," *IEEE Trans. Ind. Electron.*, vol. 57, no. 7, pp. 2527–2535, Jul. 2010.
[7] L. Zhang, H. Gao, and O. Kaynak, "Network-induced constraints in networked control systems—A survey," *IEEE Trans. Ind. Informat.*, vol. 9, no. 1, pp. 403–416, Feb. 2013.
[8] S. Deshmukh, B. Natarajan, and A. Pahwa, "Voltage/VAR control in distribution networks via reactive power injection through distributed generators," *IEEE Trans. Smart Grid*, vol. 3, no. 3, pp. 1226–1234, Sep. 2012.
[9] A. Borghetti, "Using mixed integer programming for the volt/var optimization in distribution feeders," *Electr. Power Syst. Res.*, vol. 98, pp. 39–50, May 2013.
[10] L. Yu, D. Czarkowski, and F. de Leon, "Optimal distributed voltage regulation for secondary networks with DGs," *IEEE Trans. Smart Grid*, vol. 3, no. 2, pp. 959–967, Jun. 2012.
[11] A. Y. S. Lam, B. Zhang, and D. N. Tse, "Distributed algorithms for optimal power flow problem," in *Proc. 51st IEEE Conf. Decision Control (CDC)*, 2012, pp. 430–437.
[12] P. Šulc, S. Backhaus, and M. Chertkov, "Optimal distributed control of reactive power via the alternating direction method of multipliers," arXiv:1310.5748v1, Oct. 2013, p. 10.
[13] B. Zhang, A. Y. S. Lam, A. Dominguez-Garcia, and D. Tse, "Optimal distributed voltage regulation in power distribution networks," arXiv:1204.5226v3 [math.OC], Apr. 2012.

[14] S. Bolognani, R. Carli, G. Cavraro, and S. Zampieri, "A distributed control strategy for optimal reactive power flow with power and voltage constraints," in *Proc. IEEE Int. Conf. Smart Grid Commun. (SmartGridComm)*, 2013, pp. 115–120.

[15] M. E. Baran and I. M. El-Markabi, "A multiagent-based dispatching scheme for distributed generators for voltage support on distribution feeders," *IEEE Trans. Power Syst.*, vol. 22, no. 1, pp. 52–59, Feb. 2007.

[16] A. A. Aquino-Lugo, R. Klump, and T. J. Overbye, "A control framework for the smart grid for voltage support using agent-based technologies," *IEEE Trans. Smart Grid*, vol. 2, no. 1, pp. 173–180, Mar. 2011.

[17] H. E. Z. Farag and E. F. El-Saadany, "A novel cooperative protocol for distributed voltage control in active distribution systems," *IEEE Trans. Power Syst.*, vol. 28, no. 2, pp. 1645–1656, May 2013.

[18] S. Bolognani and S. Zampieri, "A gossip-like distributed optimization algorithm for reactive power flow control," in *Proc. IFAC World Congr.*, 2011, pp. 1–14.

[19] S. Bolognani and S. Zampieri, "A distributed control strategy for reactive power compensation in smart microgrids," *IEEE Trans. Autom. Control*, vol. 58, no. 11, pp. 2818–2833, Nov. 2013.

[20] S. Bolognani *et al.*, "Distributed multi-hop reactive power compensation in smart micro-grids subject to saturation constraints," in *Proc. 51st IEEE Conf. Decision Control*, 2012, no. 257462, pp. 1118–1123.

[21] P. Tenti, A. Costabeber, P. Mattavelli, and D. Trombetti, "Distribution loss minimization by token ring control of power electronic interfaces in residential microgrids," *IEEE Trans. Ind. Electron.*, vol. 59, no. 10, pp. 3817–3826, Oct. 2012.

[22] V. Loia, A. Vaccaro, and K. Vaisakh, "A self-organizing architecture based on cooperative fuzzy agents for smart grid voltage control," *IEEE Trans. Ind. Informat.*, vol. 9, no. 3, pp. 1415–1422, Aug. 2013.

[23] Riverbed Technology. (2014). *OPNET Modeler Wireless Suite v17.1* [Online]. Available: http://support.riverbed.com/

[24] Powersys. (2014). *EMTP-RV v2.5* [Online]. Available: http://www.emtp.com/

[25] IEEE PES. (2014). *Distribution Test Feeders* [Online]. Available: http://www.ewh.ieee.org/soc/pes/dsacom/testfeeders/

[26] A. G. Phadke and J. S. Thorp, *Synchronized Phasor Measurements and Their Applications (Power Electronics and Power Systems)*. New York, NY, USA: Springer, 2008, p. 247.

[27] G. Sanchez-Ayala, J. R. Aguerc, D. Elizondo, and M. Lelic, "Current trends on applications of PMUs in distribution systems," in *Proc. IEEE PES Innov. Smart Grid Technol. Conf. (ISGT)*, 2013, pp. 1–6.

[28] A. Borghetti, C. A. Nucci, M. Paolone, G. Ciappi, and A. Solari, "Synchronized phasors monitoring during the islanding maneuver of an active distribution network," *IEEE Trans. Smart Grid*, vol. 2, no. 1, pp. 82–91, Mar. 2011.

[29] M. Paolone, A. Borghetti, and C. A. Nucci, "A synchrophasor estimation algorithm for the monitoring of active distribution networks in steady state and transient conditions," in *Proc. 17th Power Syst. Comput. Conf. (PSCC'11)*, Stockholm, Sweden, 2011, pp. 22–26.

[30] G. Kron, *Tensor Analysis of Networks*. New York, NY, USA: Wiley, 1965.

[31] F. Dörfler and F. Bullo, "Kron reduction of graphs with applications to electrical networks," *IEEE Trans. Circuits Syst. I., Reg. Papers*, vol. 60, no. 1, pp. 150–163, Jan. 2013.

[32] S. Boyd and A. Ghosh, "Randomized gossip algorithms," *IEEE Trans. Inf. Theory*, vol. 52, no. 6, pp. 2508–2530, Jun. 2006.

[33] C. Yang, G. Zhabelova, C.-W. Yang, and V. Vyatkin, "Cosimulation environment for event-driven distributed controls of smart grid," *IEEE Trans. Ind. Informat.*, vol. 9, no. 3, pp. 1423–1435, Aug. 2013.

[34] K. Hopkinson *et al.*, "EPOCHS: A platform for agent-based electric power and communication simulation built from commercial off-the-shelf components," *IEEE Trans. Power Syst.*, vol. 21, no. 2, pp. 548–558, May 2006.

[35] H. Lin, S. S. Veda, S. S. Shukla, L. Mili, and J. Thorp, "GECO: Global event-driven co-simulation framework for interconnected power system and communication network," *IEEE Trans. Smart Grid*, vol. 3, no. 3, pp. 1444–1456, Sep. 2012.

[36] T. Godfrey *et al.*, "Modeling smart grid applications with co-simulation," in *Proc. 1st IEEE Int. Conf. Smart Grid Commun.*, 2010, pp. 291–296.

[37] G. Celli, P. A. Pegoraro, F. Pilo, G. Pisano, and S. Sulis, "DMS cyber-physical simulation for assessing the impact of state estimation and communication media in smart grid operation," *IEEE Trans. Power Syst.*, Feb. 2014, to be published.

[38] A. Monti, M. Colciago, P. Conti, M. Maglio, and R. Dougal, "A co-simulation approach for analysing the impact of the communication infra-structure in power system control," in *Proc. Conf. Grand Challenges Model. Simulation (GCMS'09)*, 2009, pp. 278–282.

[39] W. Li, A. Monti, M. Luo, and R. A. Dougal, "VPNET: A co-simulation framework for analyzing communication channel effects on power systems," in *Proc. IEEE Electr. Ship Technol. Symp.*, 2011, pp. 143–149.

[40] S. C. Muller, H. Georg, C. Rehtanz, and C. Wietfeld, "Hybrid simulation of power systems and ICT for real-time applications," in *Proc. 3rd IEEE PES Innov. Smart Grid Technol. Eur. (ISGT Europe)*, 2012, pp. 1–7.

[41] D. Babazadeh, M. Chenine, K. Zhu, L. Nordström, and A. Al-Hammouri, "A platform for wide area monitoring and control system ICT analysis and development," in *Proc. IEEE Grenoble PowerTech Conf.*, 2013, pp. 1–7.

[42] M. Lévesque, D. Q. Xu, G. Joós, and M. Maier, "Communications and power distribution network co-simulation for multidisciplinary smart grid experimentations," in *Proc. SCS/ACM Spring Simul. Multi-Conf.*, 2012, pp. 1–7.

[43] D. Q. Xu, G. Joos, M. Levesque, and M. Maier, "Integrated V2G, G2V, and renewable energy sources coordination over a converged fiber-wireless broadband access network," *IEEE Trans. Smart Grid*, vol. 4, no. 3, pp. 1381–1390, Sep. 2013.

[44] J. Nutaro, P. T. Kuruganti, L. Miller, S. Mullen, and M. Shankar, "Integrated hybrid-simulation of electric power and communications systems," in *Proc. IEEE Power Eng. Soc. Gen. Meet.*, 2007, pp. 1–8.

[45] V. Liberatore and A. Al-Hammouri, "Smart grid communication and co-simulation," in *Proc. IEEE EnergyTech*, 2011, pp. 1–5.

[46] A. T. Al-Hammouri, "A comprehensive co-simulation platform for cyber-physical systems," *Comput. Commun.*, vol. 36, no. 1, pp. 8–19, 2012.

[47] S. K. Khaitan and J. D. McCalley, "Cyber physical system approach for design of power grids: A survey," in *IEEE Power Energy Soc. Gen. Meet.*, 2013, pp. 1–5.

[48] R. Bottura, A. Borghetti, F. Napolitano, and C. A. Nucci, "ICT-power co-simulation platform for the analysis of communication-based volt/var optimization in distribution feeders," in *Proc. 5th IEEE Innov. Smart Grid Technol. Conf. (ISGT'14)*, 2014, pp. 1–5.

[49] R. Bottura, D. Babazadeh, K. Zhu, A. Borghetti, L. Nordstrom, and C. A. Nucci, "SITL and HLA co-simulation platforms: Tools for analysis of the integrated ICT and electric power system," in *Proc. IEEE EURO-CON*, 2013, pp. 918–925.

[50] K. Molnár, J. Hošek, and L. Růčka, "Mutual cooperation of external application and OPNET Modeler simulation environment," in *Proc. Int. Conf. Res. Telecommun. Technol. (RTT'09)*, 2009, pp. 1–5.

[51] D. Z. Lu and H. Yang, *Unlocking the Power of OPNET Modeler*. Cambridge, U.K.: Cambridge Univ. Press, 2012.

[52] B. Khodabakhchian, "Modeling on-load tap changers in EMTP-RV," *EMTP-RV Newslett.*, vol. 1, no. 1, pp. 11–15, 2005.

[53] M. Larsson, "Coordination of cascaded tap changers using a fuzzy-rule-based controller," *Fuzzy Sets Syst.*, vol. 102, no. 1, pp. 113–123, Feb. 1999.

[54] T. Chen, M. Chen, T. Inoue, P. Kotas, and E. A. Chebli, "Three-phase cogenerator and transformer models for distribution system analysis," *IEEE Trans. Power Deliv.*, vol. 6, no. 4, pp. 1671–1681, Oct. 1991.

[55] M. Z. Kamh and R. Iravani, "Unbalanced model and power-flow analysis of microgrids and active distribution systems," *IEEE Trans. Power Del.*, vol. 25, no. 4, pp. 2851–2858, Oct. 2010.

Riccardo Bottura (S'13) was born in Ostiglia, Italy, in 1986. He received the Laurea degree in telecommunication engineering from the University of Bologna, Bologna, Italy, in 2011, where he is pursuing the Ph.D. degree in electrical engineering.

His research interests include the analysis and cosimulation of networked control systems applied to electric power distribution networks.

Alberto Borghetti (M'97–SM'03) was born in Cesena, Italy, in 1967. He received the Laurea degree (Hons.) in electrical engineering from the University of Bologna, Bologna, Italy, in 1992.

Since then, he has been working with the Power System Group at the University of Bologna, where he was appointed Researcher in 1994 and Associate Professor in 2004. His research interests include power system analysis, with particular reference to voltage collapse, power system restoration after blackout, electromagnetic transients, optimal generation scheduling, and distribution system operation. He serves as an Editor of IEEE TRANSACTIONS ON SMART GRID and is on the editorial board of *Electric Power Systems Research*.